Electronic Supplementary Information for Disentangling doping and strain effects at defects of grown MoS_2 monolayers with nano-optical spectroscopies

Frederico B. Sousa, Rafael Battistella Nadas, Rafael Martins, Ana P. M. Barboza, Jaqueline S. Soares, Bernardo R. A. Neves, Ive Silvestre, Ado Jorio, and Leandro M. Malard.

This Electronic Supplementary Information includes:

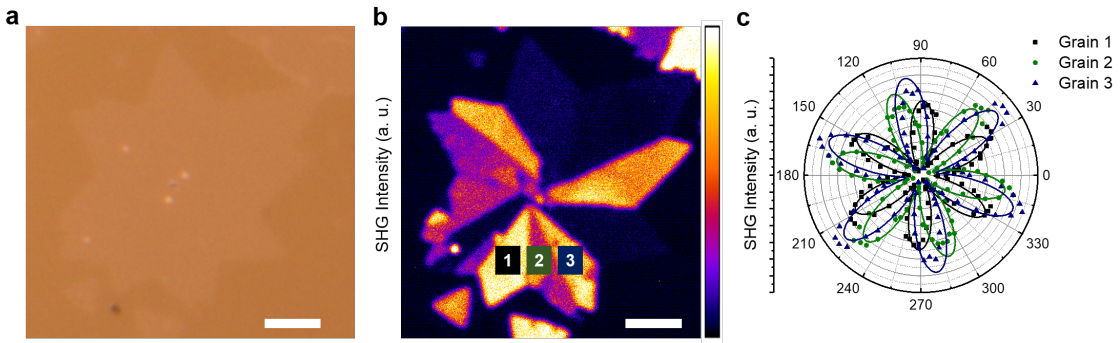

Figure S1: **a** Optical image of MoS_2 monolayer A1 sample shown in Figure 1. **b** SHG intensity image of MoS_2 monolayer A1 sample with the 3 studied grains highlighted. Scale bar: 5 μm. **c** Polarized SHG measurement for grains 1, 2 and 3 of MoS_2 monolayer A1 sample. The relative orientations between them are: $\theta_{1,2} = 21°$, $\theta_{1,3} = 11°$ and $\theta_{2,3} = 10°$.

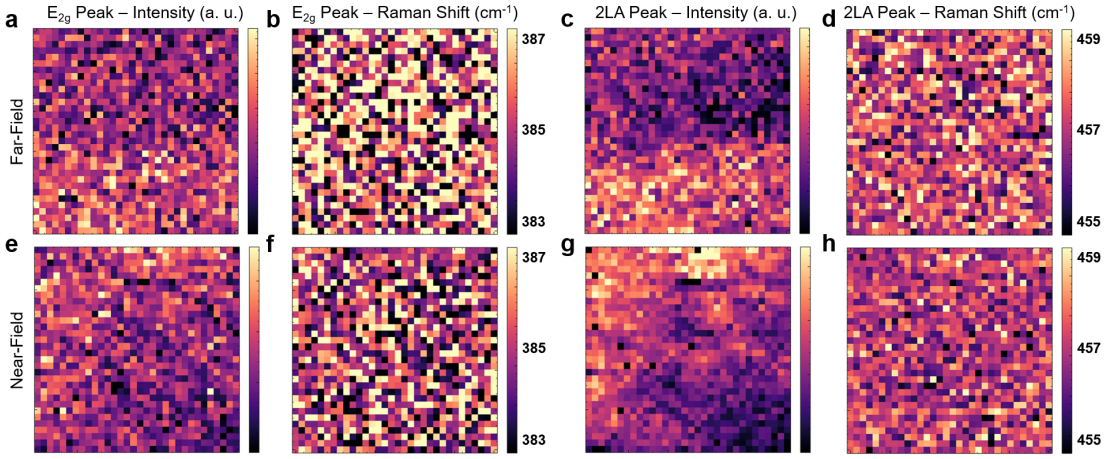

Figure S2: **a-d** Far-field E_{2g} intensity (**a**), E_{2g} frequency (**b**), 2LA intensity (**c**), and 2LA frequency (**d**) maps of MoS_2 monolayer A2 sample. **e-h** Near-field E_{2g} intensity (**e**), E_{2g} frequency (**f**), 2LA intensity (**g**), and 2LA frequency (**h**) maps of MoS_2 monolayer A2 sample. These maps are from the same region of the exciton maps of Figure 2.

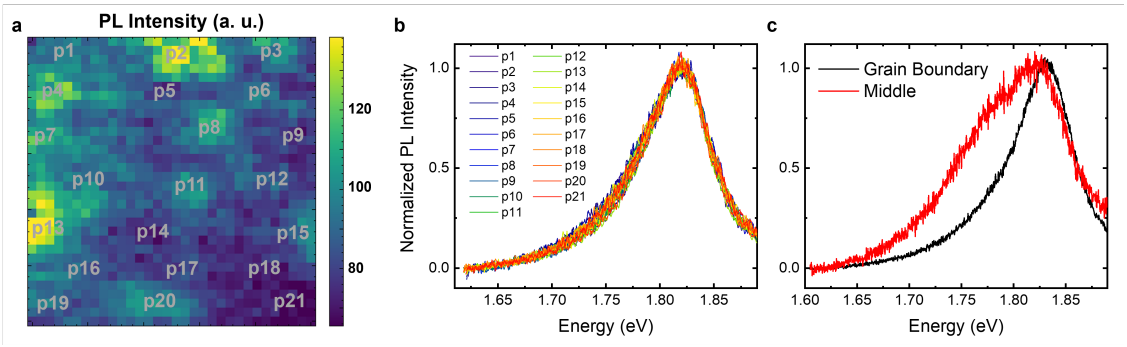

Figure S3: **a** Near-field PL intensity map from Figure 2 highlighting 21 different points selected for the PL spectral shape comparison. **b** Normalized near-field PL spectra from the 21 points shown in (**a**), which were also shifted in energy when necessery to match all their maximums. A minimal shape variation can be observed, indicating a minor contribution of doping effects. **c** Normalized near-field PL spectra from grain boundary and grain middle regions taken from Figure 1 data for comparison. A significant difference in the spectral shape is noted, confirming the strong doping effect at the grain boundary.

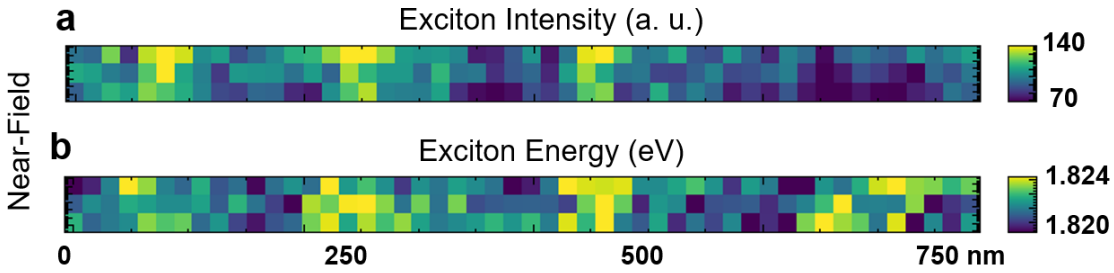

Figure S4: **a,b** Near-field exciton intensity (**a**) and exciton energy (**b**) maps of MoS_2 monolayer A2 sample showing localized strain fields in a different sample region.

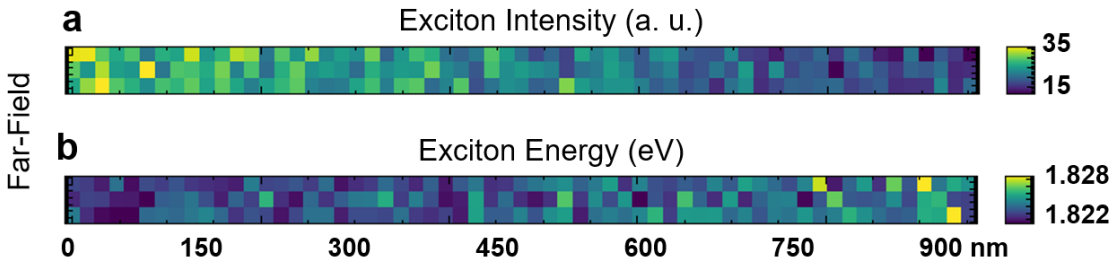

Figure S5: **a,b** Far-field exciton intensity (**a**) and exciton energy (**b**) maps at the edge of MoS_2 monolayer A2 sample showing no localized optical features. These maps are from the same region of the maps of Figure 3.

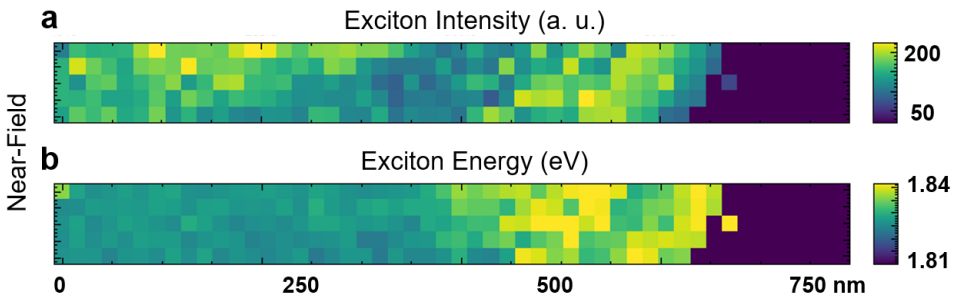

Figure S6: **a,b** Near-field exciton intensity (**a**) and exciton energy (**b**) maps in another edge region of MoS_2 monolayer A2 sample showing similar PL enhancement and blueshift features presented at the edge region of Figure 3.

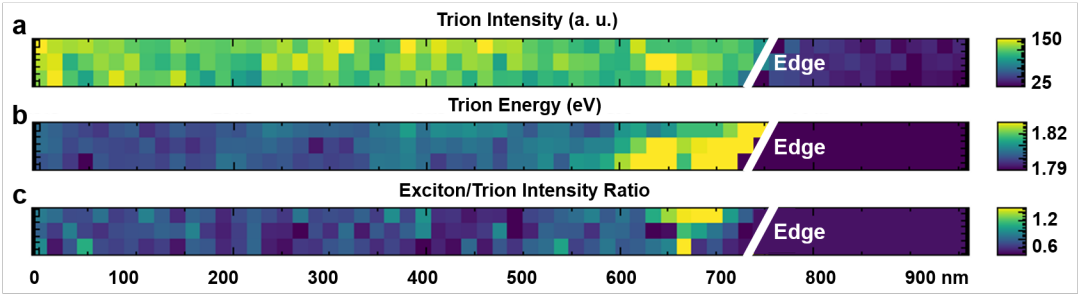

Figure S7: **a,b** NF TEPL hyperspectral maps of the trion intensity (**a**) and energy (**b**) at the same edge region of the MoS_2 monolayer shown in Figure 3. **c** Exciton/trion intensity ration map of the same edge. The similar observed blueshift of the exciton and trion emissions together with the low variation of the exciton/trion intensity ratio at the edge indicate no relevant doping effect.

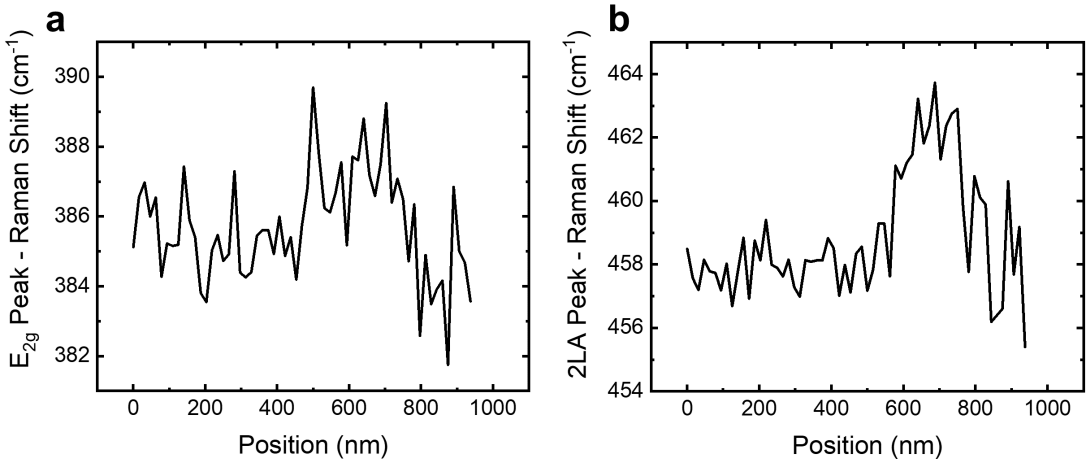

Figure S8: **a,b** E_{2g} (**a**) and 2LA (**b**) frequency profiles along the edge of MoS_2 monolayer A2 sample.

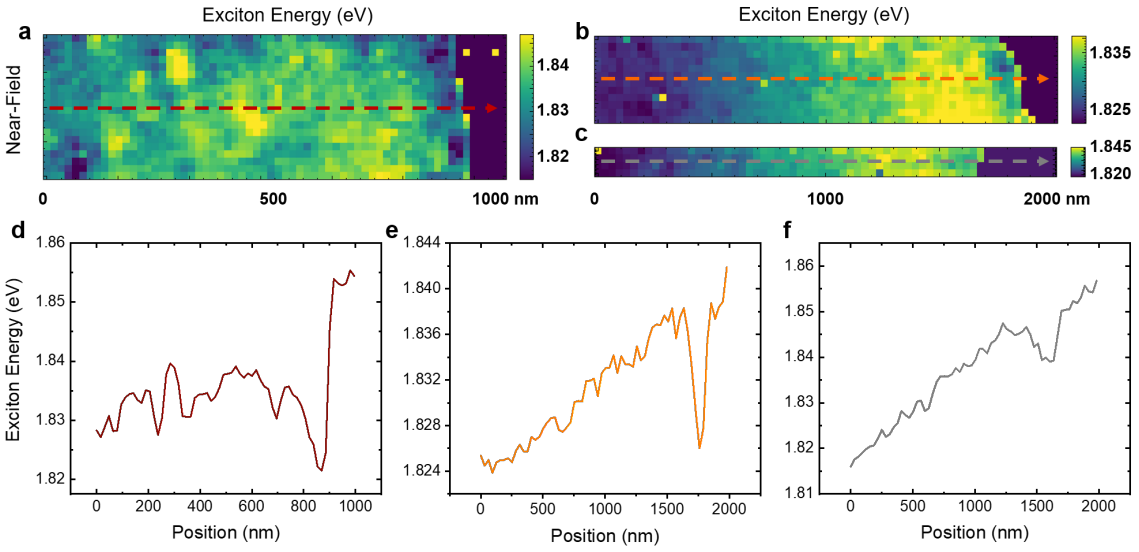

Figure S9: **a-c** Near-field exciton energy maps in other edge regions of MoS_2 monolayer A1 sample showing a similar PL redshift response presented at the edge region of Figure 4. **d-f** Exciton energy profiles along the edges of (**a-c**) highlighting the PL redshift feature. The profiles colors correspond to the dashed arrow colors of (**a-c**).

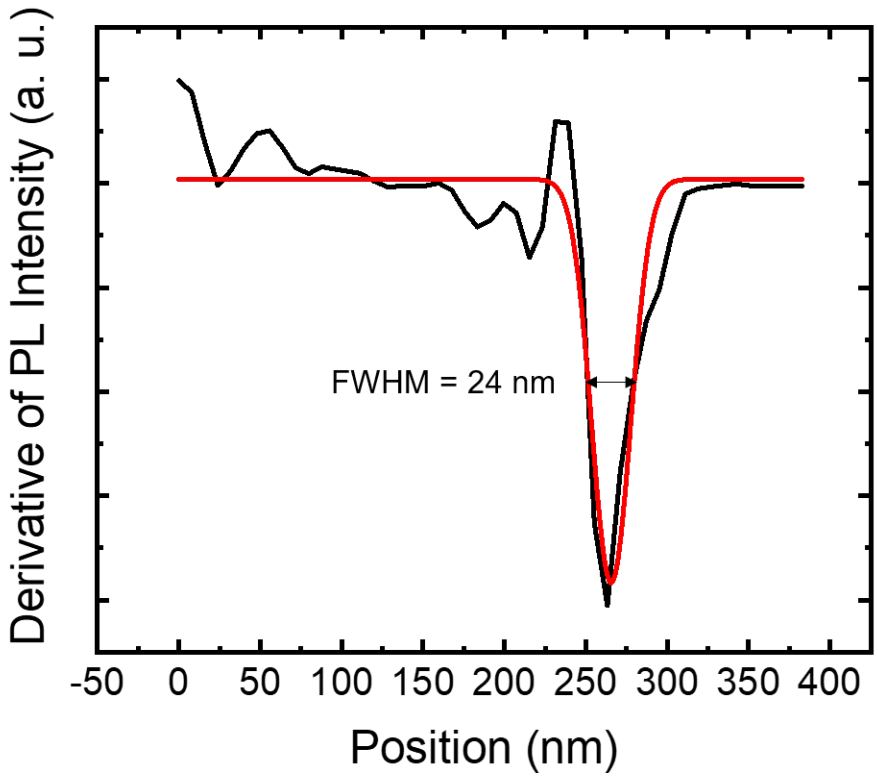

Figure S10: To extract the spatial resolution of the near-field measurements we differentiated the PL intensity profile along the edge (in black) of Figure 4 and fitted it with a Gaussian function (in red). The spatial resolution of the measurement is the fitted full width at half maximum (FWHM) = 24 nm.

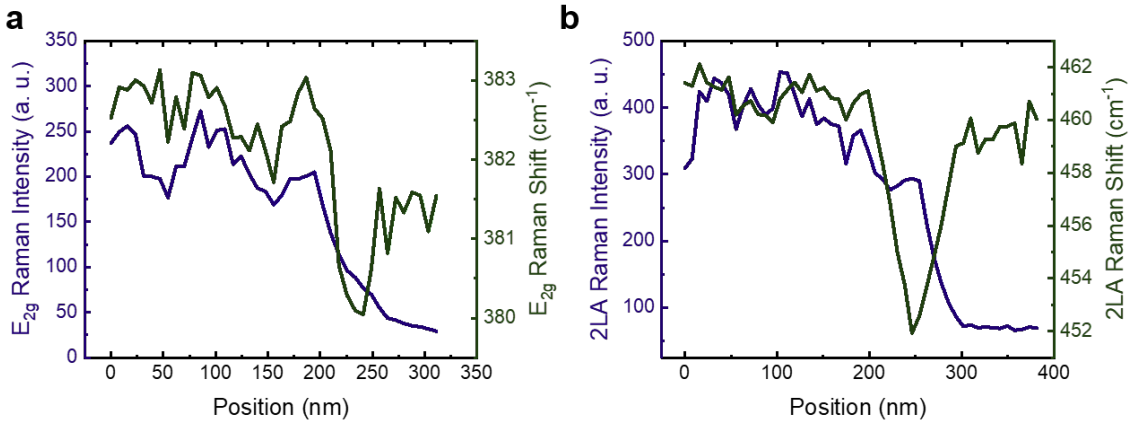

Figure S11: **a,b** E_{2g} (**a**) and 2LA (**b**) intensity and frequency profiles along the edge of MoS_2 monolayer A1 sample. These profiles were taken from the near-field Raman maps of Figure 5.